A PRECISE DETERMINATION OF THE FINE STRUCTURE CONSTANTS FOR Cr^{3+} IN RUBY

GARY D. HUTTON

A PRECISE DETERMINATION OF THE FINE STRUCTURE CONSTANTS FOR Cr^{3+} IN RUBY

****

Gary D. Hutton

A PRECISE DETERMINATION OF THE FINE STRUCTURE CONSTANTS FOR Cr^{3+} IN RUBY

by

Gary D. Hutton

Submitted in partial fulfillment of
the requirements for the degree of

MASTER OF SCIENCE
IN
PHYSICS

United States Naval Postgraduate School
Monterey, California

1965

A PRECISE DETERMINATION OF THE FINE STRUCTURE CONSTANTS FOR Cr^{3+} IN RUBY

by

Gary D. Hutton

This work is accepted as fulfilling
the thesis requirements for the degree of
MASTER OF SCIENCE
IN
PHYSICS
from the
United States Naval Postgraduate School

ABSTRACT

The aluminum oxide crystal, Al_2O_3, doped with a small amount of chromium, which is called ruby, is widely used in solid state physics research and applications. The experimental work described in this thesis is concerned with the precise determination of three important paramagnetic resonance parameters of the ruby crystal at room temperature. These are the two spectroscopic splitting factors ($g_{\parallel}$ and $g_{\perp}$) and the crystal field splitting (D) of the chromium ion energy levels.

The values obtained are: $g_{\parallel} = 1.98145 \pm .00020$, $g_{\perp} = 1.98137 \pm .00067$, $D = 5.74674 \pm .00080$ Kmc/sec.

TABLE OF CONTENTS

Section	Title	Page
1.	Introduction	1
2.	Description of Apparatus	6
3.	Experimental Procedure	11
4.	Data	14
5.	Parameter Determination	16
6.	Results	25
7.	Appendix I	28
8.	Appendix II	31
9.	Bibliography	34

LIST OF ILLUSTRATIONS

Figure		Page
1.	Magnetic Field Vector in Principle Coordinate System	2
2.	Block Diagram of Spectrometer	7
3.	Optical Allignment Setup	11
4.	Oscilloscope Display	13
5.	Energy Levels in Dimensionless Coordinates	15
6.	g Versus Angle	18
7.	Plot of Ninety Degree Computer Data	22

1. Introduction

In order to determine precisely the parameters of a given physical system, the experimentalist normally requires a precise theory describing the phenomena being observed. For paramagnetic resonance in crystals, the theory which best predicts the behavior of the spin energy levels of the paramagnetic ions in an externally applied magnetic field is the quantum mechanical spin Hamiltonian developed in the references 1, 2, 5 and 7.

The specific form of the spin Hamiltonian used here applies to an ionic crystal field of medium strength. Medium strength means that the crystal field interaction with the ion spin is stronger than its spin-orbit coupling. The Hamiltonian, used is also abbreviated. The terms for the spin-orbit interaction, nuclear spin-electron spin interaction, and other much smaller terms have been omitted. This simplified Hamiltonian is:

$$\mathcal{H} = \beta_o \vec{H} \cdot \hat{g} \cdot \vec{S} + \vec{S} \cdot \hat{D} \cdot \vec{S}$$

The first term is the external magnetic field interaction with the magnetic moment of the ion; where $\vec{H}$ is the magnetic field strength vector, $\hat{g}$ is the spectroscopic splitting factor tensor, and $\vec{s}$ is the "effective-spin" vector operator which does not necessarily have the same total eigenvalue as the free ion. The second term is the interaction energy of the crystal field with valence electrons of the ion; where $\hat{D}$ is the electrostatic field strength tensor. The constant β_o is the Bohr magneton.

The procedure followed here to find the energy eigenvalues of this Hamiltonian is to diagonalize its matrix representation. Therefore, the

development of the matrix Hamiltonian will now be roughly outlined.

The quantities in each term must first be referred to the same coordinate system. The best choice is the principal axis system of the crystal where $\hat{D}$ is diagonal. In addition, if the crystal has axial symmetry, as in the case of ruby, the z axis can be chosen to be the axis of symmetry and the x and y axes chosen arbitrarily in the perpendicular plane. In order to simplify the Hamiltonian the external field will be used to orient the axes such that $\vec{H}$ lies in the x-z plane and makes an angle θ with the z axis. See Figure 1. The Hamiltonian now becomes:

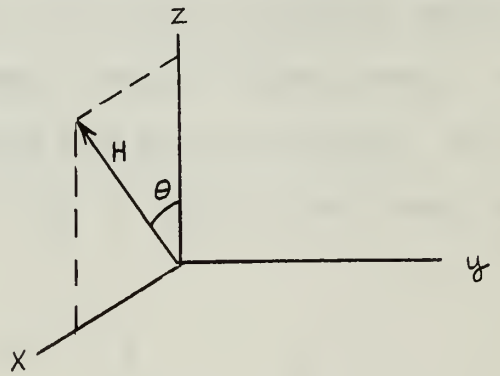

Figure 1

$$\mathcal{H} = \beta_o H \cos\theta\, g_{zz} S_z + \beta_o H \sin\theta\, g_{xx} S_x + \beta_o (0)\, g_{yy} S_y + D_{xx} S_x^2 + D_{yy} S_y^2 + D_{zz} S_z^2$$

The assumption that $\hat{g}$ is also now diagonal is valid from group theoretic arguments.

The convention now is to add a constant energy term, $-1/3(D_{xx} + D_{yy} + D_{zz})\, S\,(S + 1)$, and regroup the S^2 terms. This additive constant has the effect of placing the zero energy reference level midway between the crystal field splitting. Also since we have axial symmetry the following quantities are defined: $g_\perp \equiv g_{xx} = g_{yy}$, $g_\parallel \equiv g_{zz}$. After regrouping, the Hamiltonian is:

$$\mathcal{H} = \beta_o H \cos\theta \, g_{\parallel} \, S_z + \beta_o H \sin\theta \, g_{\perp} \, S_x + D\left(S_z^2 - 1/3 S(S+1)\right) + E(S_x^2 - S_y^2)$$

where: $D \equiv D_{zz} - 1/2(D_{xx} + D_{yy})$, $E \equiv 1/2(D_{xx} - D_{yy})$

The constant E is zero in axial symmetry since $D_{xx} = D_{yy}$.

It is found from resonance data on ruby that an external magnetic field splits the paramagnetic ion energy levels into four levels. Therefore, since the number of nondegenerate spin levels must equal $2S + 1$, then the effective spin equals $3/2$. The S matrices are, thus, the 4x4 spin $3/2$ matrices. That is:

$$\mathcal{H} = \beta_o H \cos\theta \, g_{\parallel} \begin{pmatrix} 3/2 & 0 & 0 & 0 \\ 0 & 1/2 & 0 & 0 \\ 0 & 0 & -1/2 & 0 \\ 0 & 0 & 0 & -3/2 \end{pmatrix}$$

$$+ \beta_o H \sin\theta \, g_{\perp} \begin{pmatrix} 0 & \sqrt{3}/2 & 0 & 0 \\ \sqrt{3}/2 & 0 & 1 & 0 \\ 0 & 1 & 0 & \sqrt{3}/2 \\ 0 & 0 & \sqrt{3}/2 & 0 \end{pmatrix}$$

$$+ D \left[\begin{pmatrix} 9/4 & 0 & 0 & 0 \\ 0 & 1/4 & 0 & 0 \\ 0 & 0 & 1/4 & 0 \\ 0 & 0 & 0 & 9/4 \end{pmatrix} - 1/3 \begin{pmatrix} 15/4 & 0 & 0 & 0 \\ 0 & 15/4 & 0 & 0 \\ 0 & 0 & 15/4 & 0 \\ 0 & 0 & 0 & 15/4 \end{pmatrix} \right]$$

Finally:

$$\mathcal{H} = \begin{pmatrix} 3/2\beta_o H\cos\theta g_{\parallel} + D & \sqrt{3}/2\beta_o H\sin\theta g_{\perp} & 0 & 0 \\ \sqrt{3}/2\beta_o H\sin\theta g_{\perp} & 1/2\beta_o H\cos\theta g_{\parallel} - D & \beta_o H\sin\theta g_{\perp} & 0 \\ 0 & \beta_o H\sin\theta g_{\perp} & -1/2\beta_o H\cos\theta g_{\parallel} - D & \sqrt{3}/2\beta_o H\sin\theta g_{\perp} \\ 0 & 0 & \sqrt{3}/2\beta_o H\sin\theta g_{\perp} & -3/2\beta_o\cos\theta g_{\parallel} + D \end{pmatrix}$$

Closed solutions for the eigenvalues of the matrix cannot be obtained except for the two cases $\theta = 0^o$ and $\theta = 90^o$. Therefore, these two sets of solutions were chosen as the theoretical equations for the experimental data.

The $\theta = 0^o$ case gives:

$$\mathcal{H}(0^o) = \begin{pmatrix} 3/2\beta_o H g_{\parallel} + D & 0 & 0 & 0 \\ 0 & 1/2\beta_o H g_{\parallel} - D & 0 & 0 \\ 0 & 0 & -1/2\beta_o H g_{\parallel} - D & 0 \\ 0 & 0 & 0 & -3/2\beta_o H g_{\parallel} + D \end{pmatrix}$$

Which is already diagonal; therefore the energy eigenvalues are:

$E_1 = 3/2\ \beta_o\ H\ g_{\parallel} + D$

$E_2 = 1/2\ \beta_o\ H\ g_{\parallel} - D$

$E_3 = -1/2\beta_o\ H\ g_{\parallel} - D$

$E_4 = -3/2\beta_o\ H\ g_{\parallel} + D$

The $\theta = 90^o$ case gives:

$$\mathcal{H}(90^o) = \begin{pmatrix} D & \frac{\sqrt{3}}{2}\beta_o H g_{\perp} & 0 & 0 \\ \frac{\sqrt{3}}{2}\beta_o H g_{\perp} & -D & \beta_o H g_{\perp} & 0 \\ 0 & \beta_o H g_{\perp} & -D & \frac{\sqrt{3}}{2}\beta_o H g_{\perp} \\ 0 & & \frac{\sqrt{3}}{2}\beta_o H g_{\perp} & D \end{pmatrix}$$

When this matrix is diagonalized the following energy eigenvalues are obtained:

$$E_1 = 1/2\ \beta_o H g_\perp + \sqrt{D^2 - \beta_o H D g_\perp + (\beta_o H g_\perp)^2}$$

$$E_2 = -1/2\beta_o H g_\perp + \sqrt{D^2 + \beta_o H D g_\perp + (\beta_o H g_\perp)^2}$$

$$E_3 = 1/2\ \beta_o H g_\perp - \sqrt{D^2 - \beta_o H D g_\perp + (\beta_o H g_\perp)^2}$$

$$E_4 = -1/2\beta_o H g_\perp - \sqrt{D^2 + \beta_o H D g_\perp + (\beta_o H g_\perp)^2}$$

The subscript notation has been chosen so that the 0^o and 90^o energies agree for a free ion having $D = 0$ and $g_\perp = g_{||}$.

As stated before, the Hamiltonian used here neglects some terms and assumes an electrostatic crystal field. Therefore, the proof of the accuracy of this approximate Hamiltonian in predicting the correct energy levels lies in the accuracy with which the experimental data fits the formulae. If the deviations of the data from the equations are less than the experimental errors then the theory is experimentally acceptable and the parameters obtained are accurate to within experimental error.

2. Description of Apparatus

The equipment employed to make the paramagnetic resonance measurements is, essentially, a research model of a conventional paramagnetic resonance spectrometer. It utilizes the microwave balanced bridge technique with crystal detection and heterodyne amplification of the resonance signal. Figure 2 shows a schematic representation of the system.

The microwave bridge is comprised of a "hybrid-tee" junction having four microwave arms. This junction divides the power as shown by the the arrows in figure 2. Two of the arms act as opposing loads and the remaining two are a power input arm and a signal output arm. The junction divides the input power equally between the loads and recombines both reflected signals to give a resultant output. One of the load arms is terminated by an attenuator and phase adjustor while the other is terminated by a cavity containing the ruby in a magnetic field. Consequently, if the phase and attenuation in the dummy load arm are adjusted for minimum output then any absorbtion of power in the cavity will show up as an unbalance signal. This unbalance is thus a very sensitive indiction of absorption by the ruby. Therefore, if the input frequency is held constant and the magnetic field swept through resonance conditions, an output resonance signal will be obtained. This signal is then detected by a crystal, amplified and, after rectification, displayed on an oscilloscope for measurement adjustments. Due to the method of bridge balancing, a resonance signal could be obtained which had any characteristic between pure absorptive or pure dispensive: therefore, a certain amount of skill was required to obtain the desirable absorption signal.

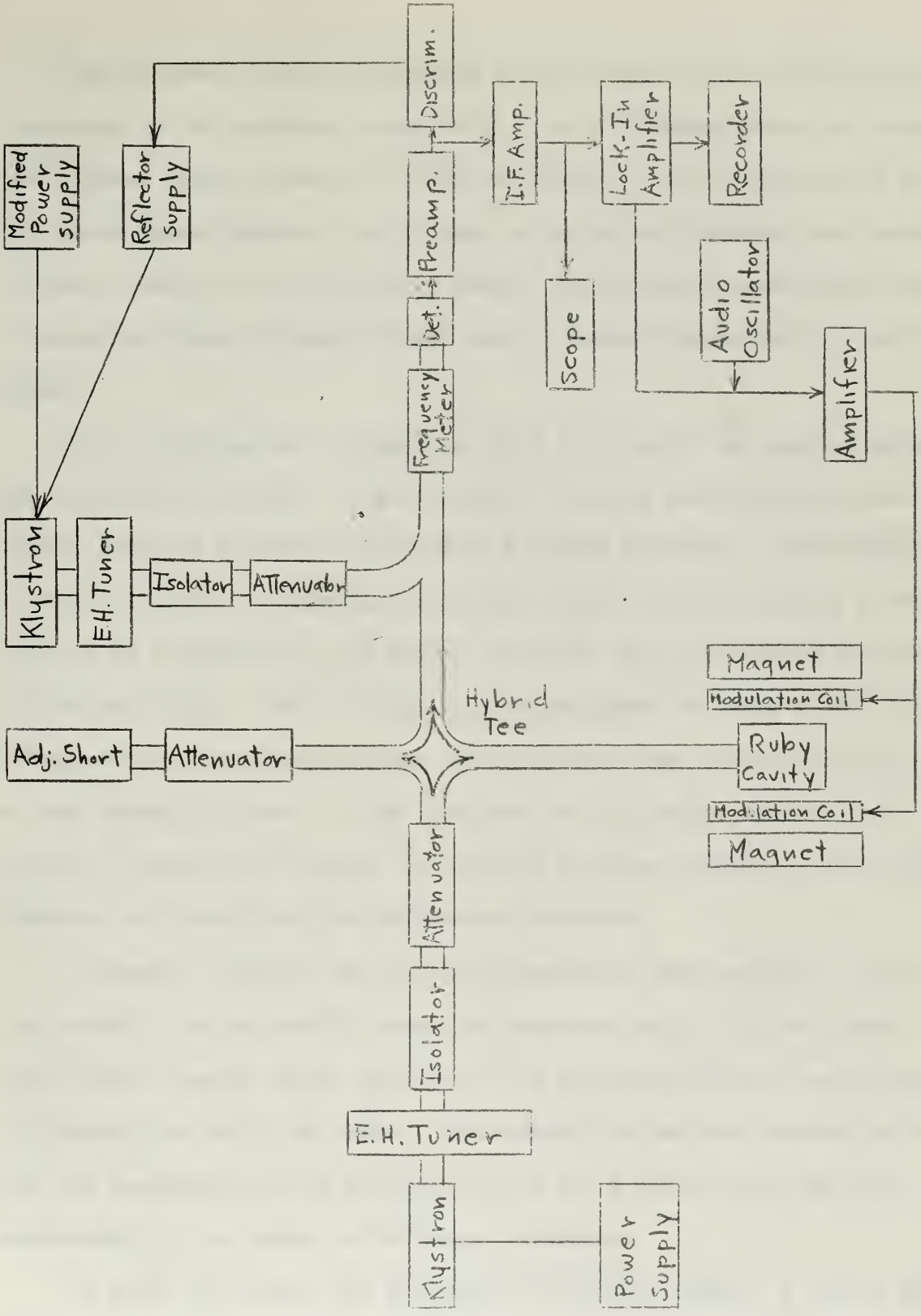

Figure 2. Block Diagram of Spectrometer

The microwave power is supplied to the bridge by a reflex klystron operating in the frequency range of 12.4 to 18 kilomegacycles per second and a power output between 50 to 100 milliwatts. The limitation on the frequency range imposed a restriction on the spread between data points. However, even over this frequency range, the different transitions gave a spread in fields strengths which nearly covered the measurable field range.

The heterodyne beat frequency, which is required for amplification of the resonance signal, is generated by coupling into the output arm of the bridge a microwave signal from a second klystron. The frequency of this klystron is locked onto the main signal so that there is a difference of 30 megacycles per second, which is the intermediate frequency of the amplifiers. This locking is a accomplished by using a 30 mc descriminator and feeding its error voltage back to the reflector voltage of the second klystron. If the frequency of the second klystron is properly located with respect to the main klystron frequency, then this feedback will stabilize the difference frequency.

Frequency stability of the main klystron is thus important, since the stability of the entire system is dependent on it. It was found that a water cooled jacket mounted on the klystron gave very good stability (about 1 mc drift per hour). This stability was good enough to permit the assumption of one frequency value for a whole series of field measurements on a number of different resonances.

In order to measure the frequency of the main signal, a cavity type frequency meter is inserted in the output arm of the bridge. This meter has a guaranteed accuracy of $\pm$ 0.1% over a wide variation in ambiant

temperature and relative humidity. However, after some preliminary data was reduced, it was found that the parameters differed from values given in other references; and the accuracy of the meter was questioned. It was, therefore, decided that a more precise frequency measurement was needed and the organic substance, diphenyl picryl hydrazyl (DPPH), was chosen as a natural paramagnetic resonance reference. DPPH has the convenient properties of an isotropic splitting factor, which is tabulated to five decimal places, and an effective spin of 1/2, which results in only one possible energy transition. The DPPH sample was about one hundreth of a gram of small crystals placed between a celluloid tape sandwich. This sample was placed in the cavity in close proximity to the ruby. Use of this natural paramagnetic resonance reference makes it possible for future investigators to check or correct the parameters obtained here.

The magnetic field is supplied by an electromagnet which has twelve inch diameter pole faces and a maximum field strength of about nine kilogauss. The magnet is mounted on a rotatable base with angular graduations, making different field orientations possible. The accompanying magnet power supply has two stages of current regulation and, therefore, has very good field stability. The pole caps of the magnet have been carefully shimmed to give a high field homogeniety; for example, at 2.5 inches of radial displacement from the center, a 3.5 kilogauss field drops 0.4 gauss. This high homogeniety insured a negligible broadening of the resonance due to inhomogeniety and allowed field measurements external to the cavity without correction for the point of measurement.

The field strength measurements were made using a nuclear spin resonance gaussmeter with a range of 0.5 to 9.0 kilogauss when a water sample is used. If an oscillator and frequency counter are used in conjunction with this gaussmeter, an accuracy of 1 part in 10^5 is possible.

As a final statement concerning the apparatus, it should be mentioned that the largest contributors to measurement uncertainty were signal noise and bridge balance drift. The signal noise was due to 60 cycle pickup and vibrations. Both of these were greatly reduced by using a direct current filament supply for the amplifiers and by mounting the entire bridge system on a vibration free platform. The bridge balance drift was minimized by constructing the dummy load arm to be as nearly alike, physically, to the cavity arm as possible.

3. Experimental Procedure

Before any measurements could be made, the ruby sample had to be correctly oriented with respect to the magnetic field. The ruby sample was in the form of 1/4 inch diameter, 1-1/8 inch long rod. The faces had been cut very carefully perpendicular to the crystal axis of symmetry and polished flat. Therefore, as an initial allignment procedure, one ruby face was used as a reference plane and its polished surface as an optical mirror. Assuming that the magnet field was perpendicular to the pole faces and knowing how much off of vertical these were, it was possible to set up a light beam system which was referred to the horizontal. A cathetometer and lamp were set up as in figure 3 and the ruby was adjusted until its face was off of vertical by the same amount as the magnet pole faces. The magnet was then rotated to a position where the ruby face and magnet pole face were approximately parallel; this being approximately a zero degree orientation. A resonance signal was now obtained on the oscilloscope and the magnet slowly rotated back and forth. The signal was seen to move to the left on the scope, reach a minimum, and move back to the right as the magnet was rotated continuously in one direction. This minimum was

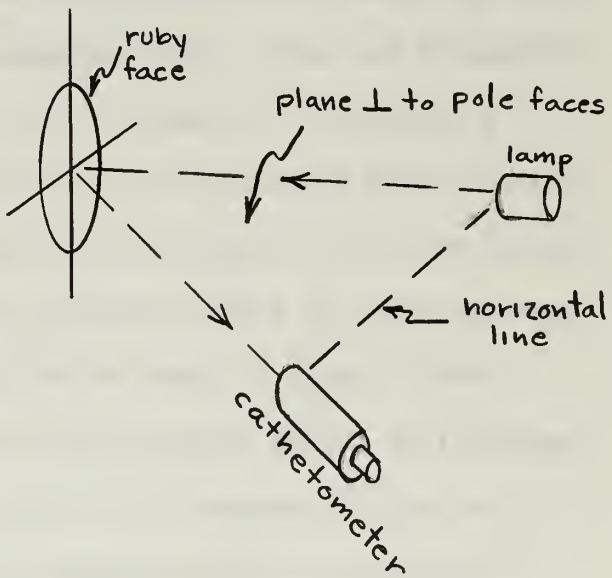

Figue 3. Optical Allignment Setup

assumed to occur when the crystal axis was correctly oriented parallel to the field. The 90 degree position could thus be obtained by rotating the magnet exactly 90 degrees from this position. The possible alignment error was less than 0.2 degrees if the assumption was correct and the ruby face had been accurately cut.

The resonance measurements were now begun. Three frequencies were used, one at the high and one at the low limits of the klystron and one about half way between. At each frequency the following transitions were measured. The two allowed zero degree transitions, $E_2 - E_3$ and $E_1 - E_2$, and four 90 degree transitions, $E_2 - E_3$, $E_1 - E_2$, $E_2 - E_4$, and $E_1 - E_3$. Also periodic measurements were made on the DPPH transition for frequency determination.

The actual signal, upon which the measurements were based, was seen as an oscilloscope display of the absorption curve. This was accomplished by taking the detected output of the final amplifier and putting it into the vertical deflection input of the oscilloscope and simultaneously putting a phase adjustable 60 cycle per second signal into the horizontal deflection input. The main field was modulated with a 60 cycle per second field having a peak to peak amplitude of about 50 gauss. Consequently, if the phase of the horizontal input signal on the oscilloscope was adjusted, a dual overlapping display of the resonance curve, as in figure 4, could be obtained. If this absorption curve was assumed to be symmetrical, then the main field could be adjusted until the zero of the modulating field, or horizontal oscilloscope input, was at the crossing of the two curves and the main field would then be at the center of the resonance. The symmetry of the absorption curve was checked by use

of a phase locked amplifier and a 37 cycle per second modulation field. The derivative curve, thus obtained, was found to be very close to symmetrical and therefore, the integral, or the absorption curve itself, was found to introduce only about ± .01% error due to asymmetry.

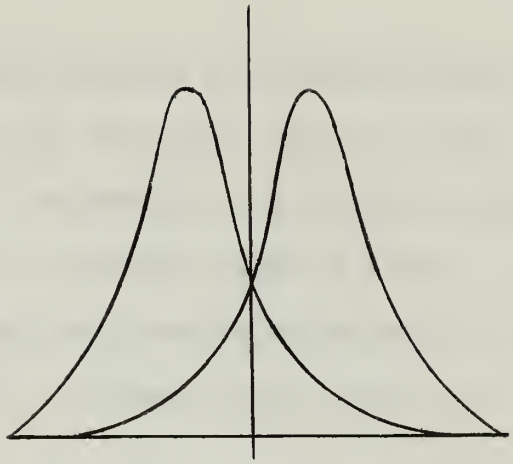

Figure 4. Oscilloscope Display

Theoretically this absorbtion curve at room temperature should be very symmetrical, but due to the method of bridge balancing, the author was not certain of his accuracy in obtaining a pure absorbtion signal and the derivative plot was needed for assurance that only a very small dispersive component was present.

When the field had been accurately set at the center of the resonance, then its strength was measured by use of the nuclear spin resonance gaussmeter. This involved accurately centering the nuclear resonance signal, as displayed on an oscilloscope, at the zero of a 60 cycle per second modulation field and measuring the frequency of the gaussmeter oscillator. This frequency was determined by beating a signal from a generator against that of the gaussmeter and counting the generator frequency when zero beat was obtained. Also at zero beat the nuclear resonance signal was again examined to guarantee that there had been no frequency shift caused by the generator signal.

This whole measurement procedure was repeated a number of times for each transition in order to obtain an estimate of the experimental uncertainty.

4. Data

In order to correlate the resonances measured to particular energy level transitions, it was necessary to plot the energy levels in dimensionless coordinates. Using dividers to determine the positions of each transitions for a constant frequency in a decending order of field strengths and, knowing approximately what the absolute scales were, it was possible to identify the resonances. The energy level plots are shown in figure 5.

The following table gives the data after averaging the repeated measurements and finding standard deviations. The values are the frequencies of the nuclear resonance gaussmeter for the magnetic field at the indicated paramagnetic resonances. The ruby used had a chromium molar percentage of 0.1%. The ambient temperature was 22 ± 2°C.

TABLE I

	Ruby resonance		DPPH resonance
$\theta = 0^\circ$	$E_2 - E_3$	$E_1 - E_2$	1/2- -1/2
	26.9164 ± .0010 mc	9.2632 ± .0005 mc	26.6087 ± .0020 mc
	23.3063 ± .0010	5.6444 ± .0005	23.0310 ± .0020
	20.6576 ± .0010	2.9840 ± .0005	20.4006 ± .0020
$\theta = 90^\circ$	$E_1 - E_3$	$E_2 - E_4$	1/2- -1/2
	(not obtained)	15.4879 ± .0008 mc	26.6087 ± .0020 mc
	4.3781 ± .0010 mc	13.1963 ± .0005	23.0310 ± .0020
	2.5264 ± .0012	11.3377 ± .0015	20.4048 ± .0015
	$E_2 - E_3$	$E_1 - E_2$	1/2- -1/2
	24.5077 ± .0010 mc	18.7616 ± .0003 mc	26.6087 ± .0020 mc
	20.4065 ± .0015	15.4376 ± .0015	23.0310 ± .0020
	17.1962 ± .0015	13.0880 ± .0010	20.4006 ± .0020

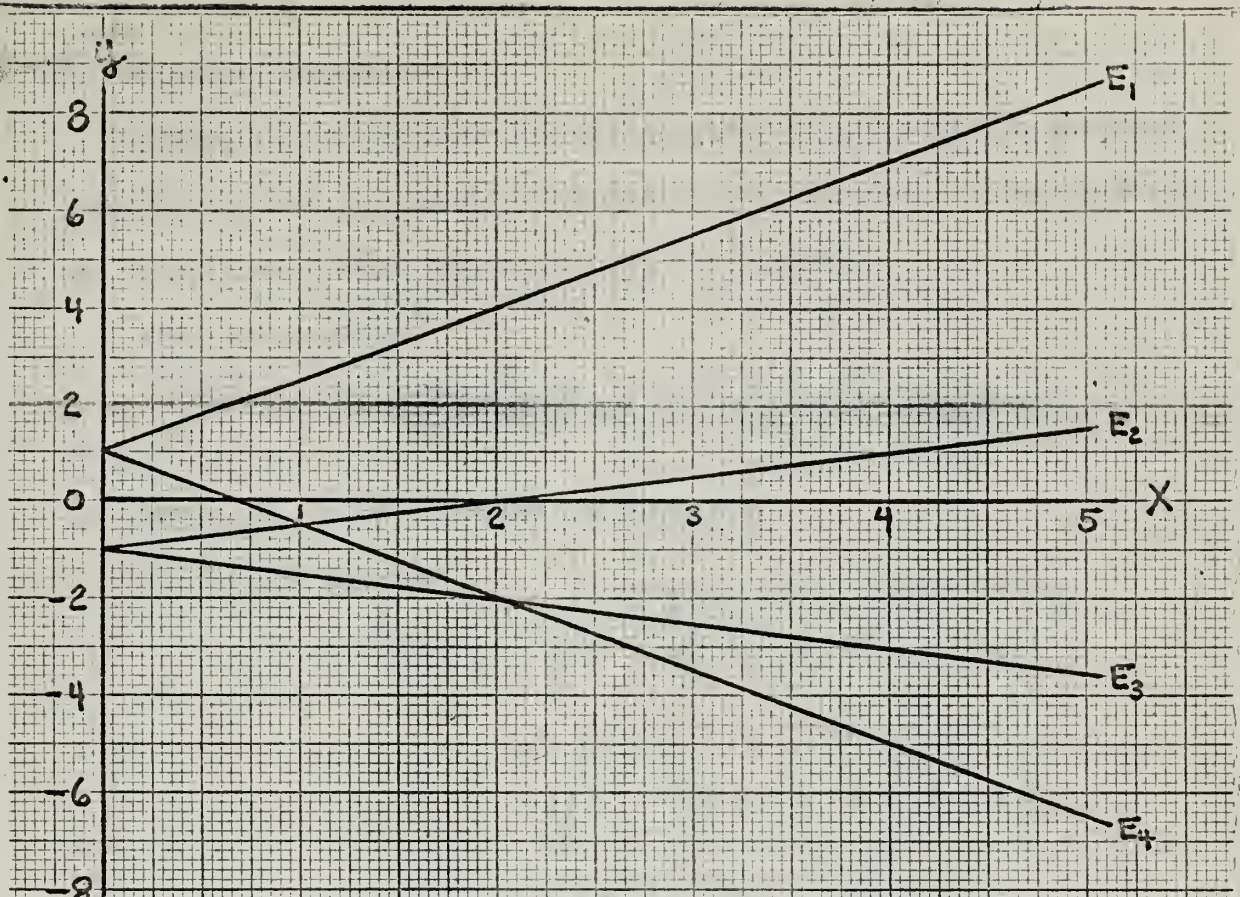

Zero Degrees ($X = \beta_o H g_{\parallel}/D$, $y = E/D$)

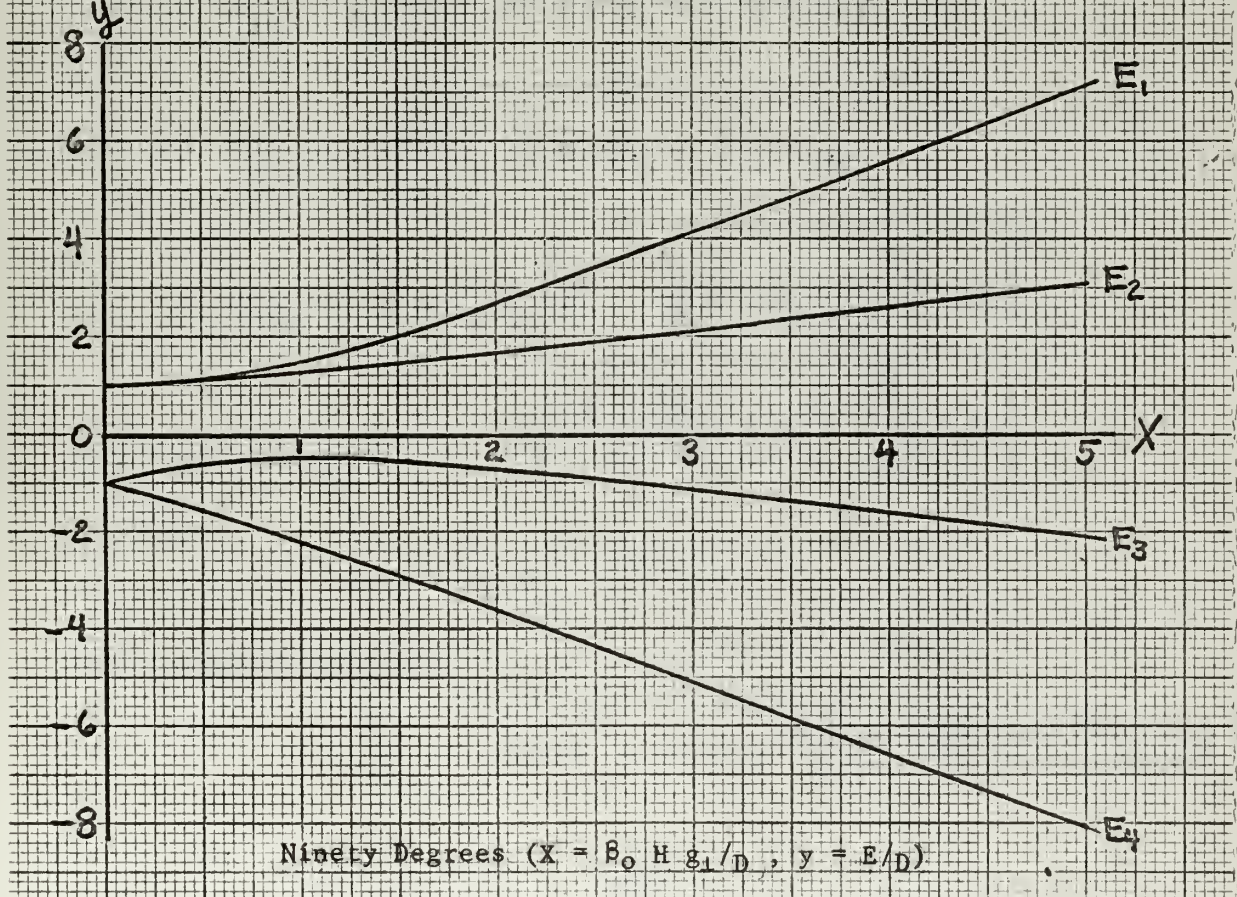

Ninety Degrees ($X = \beta_o H g_{\perp}/D$, $y = E/D$)

Figure 5: Energy Levels in Dimensionless Coordinates

5. Parameter Determination

Taking the differences of the energies, as given in the introduction, and dividing by planck's constant (h), the desired frequencies of the transitions, which were measured, are obtained.

For zero degrees:

$$\nu_{2-3} = \frac{\beta_o}{h} H g_{\parallel} \quad ; \quad \nu_{1-2} = \frac{\beta_o}{h} H g_{\parallel} + 2D$$

Where D is now in units of frequency

For ninety degrees:

$$\nu_{2-3} = -\frac{\beta_o}{h} H g_{\perp} + \sqrt{D^2 + \frac{\beta_o}{h} H D g_{\perp} + \left(\frac{\beta_o}{h} H g_{\perp}\right)^2} + \sqrt{D^2 - \frac{\beta_o}{h} H D g + \left(\frac{\beta_o}{h} H g_{\perp}\right)^2}$$

$$\nu_{1-3} = 2\sqrt{D^2 - \frac{\beta_o}{h} H D g_{\perp} + \left(\frac{\beta_o}{h} H g_{\perp}\right)^2}$$

$$\nu_{2-4} = 2\sqrt{D^2 + \frac{\beta_o}{h} H D g_{\perp} + \left(\frac{\beta_o}{h} H g_{\perp}\right)^2}$$

$$\nu_{1-2} = \frac{\beta_o}{h} H g_{\perp} + \sqrt{D^2 - \frac{\beta_o}{h} H D g_{\perp} + \left(\frac{\beta_o}{h} H g_{\perp}\right)^2} - \sqrt{D^2 + \frac{\beta_o}{h} H D g_{\perp} + \left(\frac{\beta_o}{h} H g_{\perp}\right)^2}$$

For DPPH:

$$\nu = \frac{\beta_o}{h} H g$$

The constants used are:

$$\frac{\beta_o}{h} = 1.39966 \pm .00004 \ \frac{\text{mc/sec}}{\text{gauss}}$$ (American Institude of Physics Handbook)

$$g = 2.00354 \pm .00003 \text{ (Reference 6)}$$

Also since the field was measured in terms of the proton resonance frequency in water, the following was used:

$$H(\text{gauss}) = (234.861 \pm .010)\ \nu_p \text{ (mc/sec)}$$

Inserting the constants and using only proton frequencies for DPPH fields and ruby fields, for the same microwave frequency, the zero degree equations are solved for $g_{\parallel}$ and D.

$$\text{for } (E_2 - E_3): \quad g_{\parallel} = (2.00354 \pm .00003)\ \frac{\nu_p \text{ (DPPH)}}{\nu_p \text{ (ruby)}}$$

$$\text{for } (E_1 - E_2): \quad D = (329.308 \pm .020)\ \left(\nu_p(\text{DPPH}) - \frac{g_{\parallel}}{g}\ \nu_p \text{ (ruby)}\right)$$

For the 90° frequency equations the following substitutions are made:

$$A \equiv \frac{\beta_o H}{h} = (328.726 \pm .020)\ \nu_p \text{ (ruby)}$$

$$B \equiv \nu_{i-j} = (658.615 \pm .040)\ \nu_p \text{ (DPPH)}$$

and the equations were solved for D as a function of $g_{\perp}$, A and B.

$$\text{for } (E_2 - E_3): \quad D = \frac{(B + Ag_{\perp})}{2}\ \sqrt{\frac{B(2Ag_{\perp} + B) - 3(Ag_{\perp})^2}{B(2Ag_{\perp} + B)}}$$

$$\text{for } (E_1 - E_3): \quad D = \frac{1}{2}\left(\sqrt{B^2 - e(Ag_{\perp})^2} - Ag_{\perp}\right)$$

$$\text{for } (E_2 - E_4): \quad D = \frac{1}{2}\left(\sqrt{B^2 - 3(Ag_{\perp})^2} + Ag_{\perp}\right)$$

$$\text{for } (E_1 - E_2): \quad D = \frac{(B - Ag_{\perp})}{2}\ \sqrt{\frac{B(2Ag_{\perp} - B) + 3(Ag_{\perp})^2}{B(2Ag - B)}}$$

a) Zero Degree Solutions

Inserting the data for the $E_2 - E_3$ transitions into the g_{11} equation, the following values were obtained.

$$g_{11} = 1.9806 \pm .0002 \quad \text{for} \quad \upsilon_{2-3} = 17.525 \text{ Kmc/sec}$$

$$g_{11} = 1.9799 \pm .0002 \quad \text{for} \quad \upsilon_{2-3} = 15.169 \text{ Kmc/sec}$$

$$g_{11} = 1.9786 \pm .0002 \quad \text{for} \quad \upsilon_{2-3} = 13.436 \text{ Kmc/sec}$$

These values do not agree within experimental error and there is an evident frequency correlation. This frequency correlation suggests a misallignment of the ruby axis and the magnetic field. In order to estimate the amount of misallignment, data from a previous run, in which a frequency meter was used, is plotted. (See figure 6) This data is from measurements of an $E_2 - E_3$ transition, at 13.597 Kmc/sec as a function of angle about zero degrees. The crystal was a different one from that used here and had a chromium percentage of .05%, therefore, the misallignment encountered here is a cutting error of the 0.1% Cr crystal face. The data has been reduced in the form of g values, obtained using the zero degree equation, versus angle from zero.

0° $\quad g = 1.9811 \pm .0010$

$\pm 1^\circ$ $\quad g_1{}^\circ = 1.9790 \pm .0010$

$\pm 2^\circ$ $\quad g_2{}^\circ = 1.9727 \pm .0010$

$\pm 3^\circ$ $\quad g_3{}^\circ = 1.9643 \pm .0010$

$\pm 4^\circ$ $\quad g_4{}^\circ = 1.9517 \pm .0010$

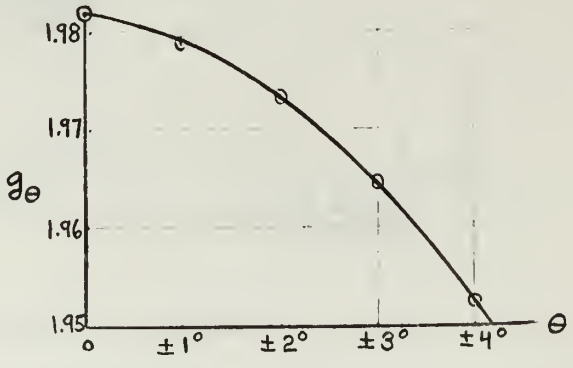

Figure 6. g versus angle

The accuracy of this data is not as good as the present data but is still useful. The curve closely fits a parabola having the formula:

$$g_\theta \simeq g_{\parallel} - (.0020)\ \theta^2 = 1.9811 - (.0020)\ \theta^2$$

Where θ is in degrees.

Comparing the value obtained at 13.436 Kmc/sec to this gives an angle of: $\theta \simeq 1.25^o$.

Rather than attempt to allign the ruby more accurately, another approach was used. Since the data obtained is accurate for some small angle approximately equal to one degree, the energies of the zero degree Hamiltonian are modified to take into account a small angle from zero. The approach is to take the general Hamiltonian, substitute θ for $\sin\theta$ and $(1-\theta^2/2)$ for $\cos\theta$ and use perturbation theory on the resultant Hamiltonian. See Appendix I for the derivation of these small angle energies. The equations for $g_{\parallel}$ and D are put in an approximate form in order to use iterative techniques. It is assumed that $g_\perp = g_{\parallel} \equiv g_0$ in the correction terms.

$$g_{\parallel} = \frac{h\nu_{2-3}}{\beta_o H} + \frac{3}{2} g_o \left(\frac{1}{1 - \left(\frac{2\ D\ h}{\beta_o g_o H}\right)^2} - 1 \right) \theta^2$$

$$D = \frac{1}{2} \left[\nu_{1-2} - g_{\parallel} \frac{\beta_o}{h} H + \frac{3}{2} g_o \frac{\beta_o}{h} H \left(1 - \frac{1}{1 + \left(\frac{2\ D\ h}{\beta_o g_o H}\right)} \right) \theta^2 \right]$$

From the previous data a $g_{\parallel} = 1.9813$ was obtained; therefore, this is used for the g_o value. Also if the present data is used in the zero degree equations for D , the values obtained do not show any misallign-

ment effect and an average value $D = 5.7462$ Kmc/sec is obtained. This is used in the small angle equations in the correction term.

Using the $E_2 - E_3$ data, the g_{II} equations are:

(1) $g_{II} = (1.98064 \pm .00020) + (2.2397)\ \theta^2$ for $\upsilon_{2-3} = 17.525$ Kmc/sec

(2) $g_{II} = (1.97988 \pm .00020) + (3.9914)\ \theta^2$ for $\upsilon_{2-3} = 15.169$ Kmc/sec

(3) $g_{II} = (1.97861 \pm .00020) + (8.0195)\ \theta^2$ for $\upsilon_{2-3} = 13.436$ Kmc/sec

At this point it is interesting to note that the constant $8.0195/\text{rad}^2$ in equation (3) is $.00243/\text{deg}^2$ and compares nicely with the experimentally obtained value of $.0020/\text{deg}^2$, which was for $\upsilon_{2-3} = 13.597$ Kmc/sec.

Now, there are three equations and two unknowns g_{II} and θ; therefore, three values of g_{II} can be obtained for an averaged value of θ. The average value of θ is:

$$\theta^2 = .0003668 \pm .0000500 \text{ radians}^2$$

or $$\theta = 1.097 \pm .080 \text{ degrees}$$

from (1) $g_{II} = 1.98146 \pm .00020$

(2) $g_{II} = 1.98134 \pm .00020$

(3) $g_{II} = 1.98155 \pm .00020$

The average of these three is:

$$\boxed{g_{II} = 1.98145 \pm .00020}$$

Using this value of g_{II} in the D equations, the same process can be used.

(4) $D = (5.74565 \pm .00080) + (2.9673)\ \theta^2$

(5) $D = (5.74605 \pm .00080) + (2.1677)\ \theta^2$

(6) $D = (5.74625 \pm .00080) + (1.2469)\ \theta^2$

The average angle is:

$\theta^2 = .0003554 \pm .0001300$ rad^2

$\theta = 1.080 \pm 0.20$ degrees

from (4) $D = 5.74670 \pm .00080$ Kmc/sec

(5) $D = 5.74682 \pm .00080$ Kmc/sec

(6) $D = 5.74669 \pm .00080$ Kmc/sec

The average of these three is:

$$\boxed{D = 5.74674 \pm .00080 \text{ Kmc/sec}}$$

b) Ninety Degree Solutions

The determination of $g_\perp$ and D from the ninety degree equations is more involved than the simple solution of a set of linear algebraic equations like the zero degree equations. The ninety degree equations are a set of quadratic algebraic equations. Using the available data there are eleven equations and the two unknown parameters. One could assume the same D value as already obtained from the zero degree data but this would not allow an independent check of the accuracy of the ninety degree equations. Therefore, the equations were solved simultaneously using the following method. If eleven simultaneous equations in two unknowns are solved, fifty five intersection values are obtained. Since this is a lengthy procedure the D equations were programmed in an IBM 1604 computer and the values of D for each of the eleven equations at values of $g_\perp$, running from 1.970 to 2.000 in steps of .001, were determined. An index i was used to label the data sets and j the

values of $g_\perp$. The values $i = 1,2,3$ are for $E_1 - E_2$ data, $i = 4,5,6$ for $E_2 - E_3$ data, $i = 7,8,9$ for $E_2 - E_4$ data, and $i = 10,11,12$ for $E_1 - E_3$ data. Where each triplet is started with the low value of B_i and increased with i . The computer was instructed to label each column of D_{ij} values as $D(i)$. Table II gives the program print out. There was no data for $i = 10$ and the zeros were printed if the value of D_{ij} was imaginary. If this data is plotted as in figure 7, the scattering of the intersection points can be seen. The results are better than this plot suggests since each intersection does not carry the same weight in determination of $g_\perp$ and D average. This is because data error gives the lines a certain width and thus the intersection coordinates are affected not only by this width but by the angle between the lines at intersection and their orientation with respect to the $g_\perp$ and D coordinate axes. Appendix II gives the derivation of the weighting factor formulae which were used in the averaging. The values of D and $g_\perp$ at each intersection were determined by locating the interval between which the two curves intersect, in Table II, and using straight line proportionality between the four D points.

The final results are given in the next section.

G	D1	D2	D3	D4	D5	D6
1.970000	5.845222	5.837711	5.849504	5.898652	5.847036	5,822137
1.971000	5.836665	5.829438	5.841004	5.885818	5.838501	5.816448
1.972000	5.828119	5.821181	5.832527	5.872942	5.829943	5.810746
1.973000	5.819585	5.812939	5.824071	5.860023	5.821363	5.805032
1.974000	5.811062	5.804713	5.815637	5.847060	5.812760	5.799305
1.975000	5.802550	5.796502	5.807225	5.834053	5.804134	5.793566
1.976000	5.794050	5.788307	5.798833	5.821003	5.795485	5.787815
1.977000	5.785561	5.780127	5.790463	5.807908	5.786813	5.782049
1.978000	5.777083	5.771962	5.782114	5.794768	5.778118	5.776271
1.979000	5.768617	5.763813	5.773786	5.781584	5.769399	5.770481
1.980000	5.760161	5.755678	5.765478	5.768354	5.760657	5.764678
1.981000	5.751717	5.747559	5.757191	5.755079	5.751892	5.758862
1.982000	5.743283	5.739454	5.748925	5.741757	5.743103	5.753033
1.983000	5.734860	5.731364	5.740679	5.728390	5.734290	5.747191
1.984000	5.726449	5.723289	5.732453	5.714976	5.725454	5.741337
1.985000	5.718048	5.715228	5.724247	5.701515	5.716593	5.735469
1.986000	5.709657	5.707182	5.716061	5.688007	5.707708	5.729588
1.987000	5.701278	5.699150	5.707895	5.674451	5.698800	5.723695
1.988000	5.692909	5.691133	5.699748	5.660847	5.689866	5.717788
1.989000	5.684550	5.683130	5.691621	5.647196	5.680909	5.711868
1.990000	5.676202	5.675141	5.683514	5.633495	5.671927	5.705934
1.991000	5.667865	5.667166	5.675426	5.619745	5.662920	5.699988
1.992000	5.659538	5.659205	5.667357	5.605947	5.653889	5.694028
1.993000	5.651221	5.651258	5.659307	5.592098	5.644832	5.688055
1.994000	5.642915	5.643325	5.651276	5.578199	5.635751	5.682068
1.995000	5.634619	5.635406	5.643264	5.564250	5.626644	5.676068
1.996000	5.626333	5.627501	5.635271	5.550250	5.617512	5.670054
1.997000	5.618057	5.619609	5.627296	5.536198	5.608355	5.664027
1.998000	5.609792	5.611731	5.619340	5.522095	5.599172	5.657986
1.999000	5.601536	5.603866	5.611402	5.507940	5.589963	5.651932

G	D7	D8	D9	D11	D12
1.970000	6.169410	5.931498	5.843850	5.758443	5.750374
1.971000	6.138282	5.916813	5.836245	5.757297	5.749804
1.972000	6.106093	5.901945	5.828593	5.756151	5.749233
1.973000	6.072736	5.886888	5.820894	5.755004	5.748663
1.974000	6.038090	5.871634	5.813148	5.753857	5.748092
1.975000	6.002004	5.856179	5.805353	5.752710	5.747521
1.976000	5.964301	5.840515	5.797509	5.751562	5.746950
1.977000	5.924763	5.824635	5.789615	5.750415	5.746380
1.978000	5.883115	5.808531	5.781671	5.749267	5.745809
1.979000	5.839009	5.792195	5.773676	5.748119	5.745237
1.980000	5.791987	5.775619	5.765629	5.746970	5.744666
1.981000	5.741429	5.758792	5.757530	5.745822	5.744095
1.982000	5.686456	5.741706	5.749377	5.744673	5.743524
1.983000	5.625751	5.724349	5.741170	5.743524	5.742952
1.984000	5.557172	5.706710	5.732908	5.742375	5.742381
1.985000	5.476772	5.688778	5.724590	5.741225	5.741809
1.986000	5.375481	5.670538	5.716216	5.740075	5.741237
1.987000	5.216465	5.651978	5.707784	5.738925	5.740666
1.988000	.000000	5.633082	5.699294	5.737775	5.740094
1.989000	.000000	5.613834	5.690744	5.736624	5.739522
1.990000	.000000	5.594216	5.682135	5.735474	5.738950
1.991000	.000000	5.574209	5.673464	5.734322	5.738378
1.992000	.000000	5.553791	5.664731	5.733171	5.737806
1.993000	.000000	5.532941	5.655935	5.732020	5.737233
1.994000	.000000	5.511632	5.647074	5.730868	5.736661
1.995000	.000000	5.489837	5.638149	5.729716	5.736089
1.996000	.000000	5.467525	5.629157	5.728564	5.735516
1.997000	.000000	5.444662	5.620097	5.727411	5.734944
1.998000	.000000	5.421210	5.610969	5.726258	5.734371
1.999000	.000000	5.397127	5.601770	5.725105	5.733798

TIME, 0 MINUTES AND 14 SECONDS

Table II: Data Print out for Ninety Degree Solutions

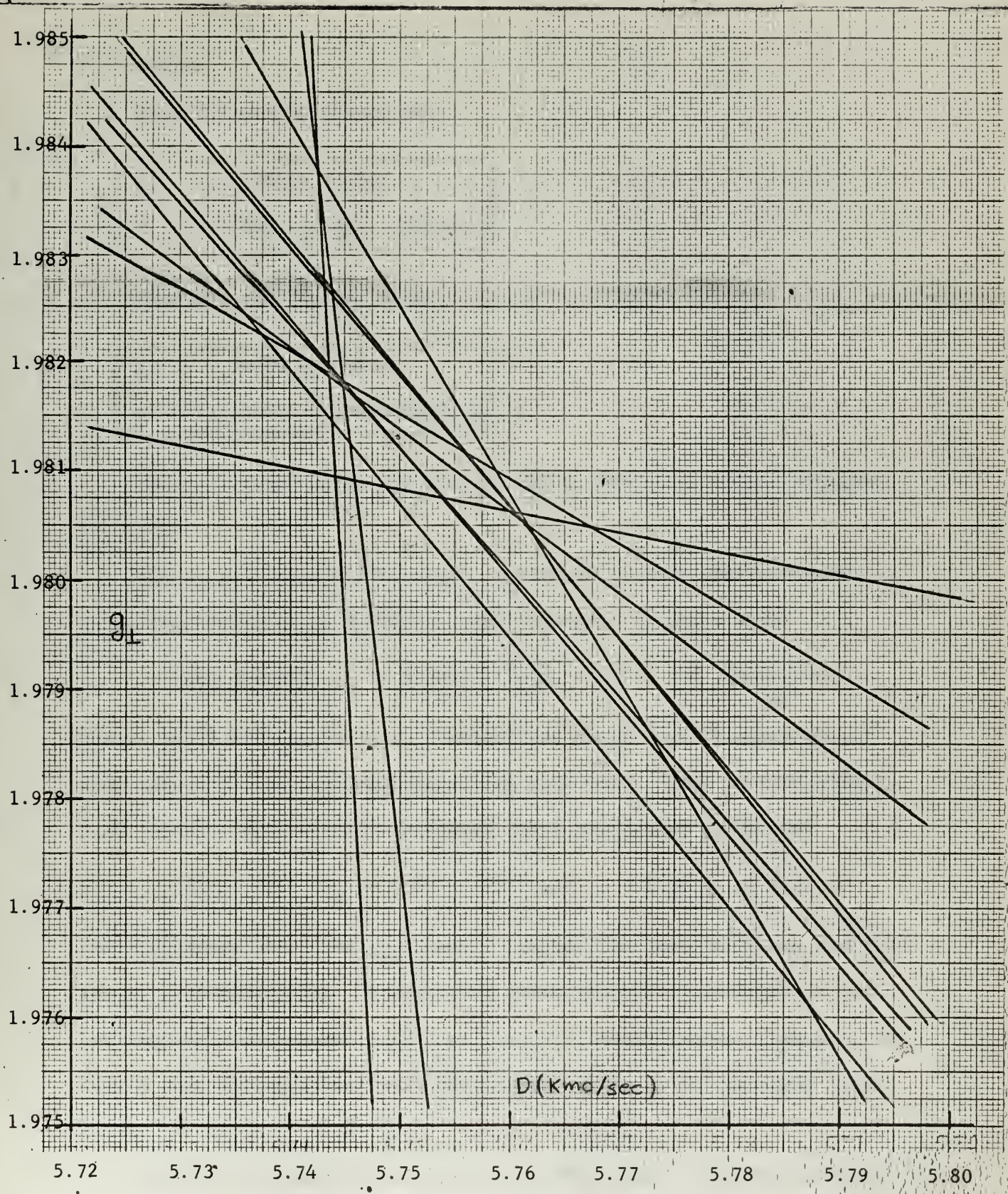

Figure 7: Plot of Ninety Degree Computer Data

6. Results

From the ninety degree data:

$$g_{\perp} = 1.98137 \pm .00067$$
$$D = 5.7489 \pm .0061 \text{ Kmc/sec}$$

From the zero degree data:

$$g_{\parallel} = 1.98145 \pm .00020$$
$$D = 5.74674 \pm .00080 \text{ Kmc/sec}$$

The D values agree and the g values are equal within experimental error.

These g values differ quite significantly from those obtained by A.A. Manenkov and A.M. Prokhorov (see reference 4) which were $g_{\parallel} = 1.9840 \pm .0006$, $g_{\perp} = 1.9867 \pm .0006$ and $D = 5.732$ Kmc/sec. Their report did not explain in detail how these were obtained except that they used the same Hamiltonian as used here. Also another author, J. E. Geusic (reference 3), measured these parameters and gives: $g_{\parallel} = 2.003 \pm .006$, $g_{\perp} = 2.00 \pm 0.02$ and $D = 5.78 \pm .03$ Kmc/sec which disagrees with the $g_{\parallel}$ and D of Manenkov and Prokhorov and also the $g_{\parallel}$ obtained here. Geusic used essentially the same Hamiltonian and similarly measured his data at zero and ninety degrees. However he stated that his agreement with calculated values at 90° was only good to 1% .

In order to check the accuracy with which the calculated values of the resonance frequencies fits the experimental values, the following tables were compiled using the g values obtained and the best D value.

(All frequencies are in Kilomegacycles per second)

$\theta = 1.10 \pm .08^{o}$

transition	(calculated)	(measured)
2-3	$17.525 \pm .002$	$17.525 \pm .002$
	$15.169 \pm .002$	$15.169 \pm .002$
	$13.435 \pm .003$	$13.436 \pm .002$
1-2	$17.525 \pm .002$	$17.525 \pm .002$
	$15.168 \pm .002$	$15.169 \pm .002$
	$13.436 \pm .002$	$13.436 \pm .002$

$\theta = 90^{0}$

transition	(calculated)	(measured)
4-3	$17.525 \pm .001$	$17.525 \pm .002$
	$15.171 \pm .001$	$15.169 \pm .002$
	$13.432 \pm .001$	$13.436 \pm .002$
3-2	$17.523 \pm .001$	$17.525 \pm .002$
	$15.168 \pm .001$	$15.169 \pm .002$
	$13.428 \pm .002$	$13.436 \pm .002$
3-1	$17.529 \pm .002$	$17.525 \pm .002$
	$15.167 \pm .001$	$15.169 \pm .002$
	$13.434 \pm .002$	$13.439 \pm .002$
4-2	$15.172 \pm .002$	$15.169 \pm .002$
	$13.445 \pm .002$	$13.439 \pm .002$

The agreement is very good for the small angle values, but the ninety degree values show a maximum disagreement of .06% which is slightly outside of the estimated experimental error. This disagreement could

possibly be caused by a misallignment at ninety degrees or an actual theoretical disagreement. An approximate perturbation Hamiltonian can be obtained for a small angle from 90^{o} but the calculations are much more tedious than for the zero degree case. Regardless of the source of the disagreement, the $g_{\perp}$ value obtained by a more accurate method would probably not vary from the value obtained here by more than approximately 0.1% .

APPENDIX I

Small Angle Hamiltonian and Energies

$$\mathcal{H} = \begin{pmatrix} 3/2\,\beta_o g_{\parallel} H(1-\theta^2/2)+D & \sqrt{3}/2\,\beta_o g_{\perp} H\theta & 0 & 0 \\ \frac{\sqrt{3}}{2}\beta_o g_{\perp} H\theta & \frac{1}{2}\beta_o g_{\parallel} H(1-\theta^2/2)-D & \beta_o g_{\perp} H\,\theta & 0 \\ 0 & \beta_o g_{\perp} H\theta & -\frac{1}{2}\beta_o g_{\parallel} H(1-\theta^2/2)-D & \frac{\sqrt{3}}{2}\beta_o g_{\perp} H\theta \\ 0 & 0 & \frac{\sqrt{3}}{2}\beta_o g_{\perp} H\theta & -\frac{3}{2}\beta_o g_{\parallel} H(1-\theta^2/2)+D \end{pmatrix}$$

Where the following substitutions were made:

$$\cos\theta = 1 - \theta^2/2 \qquad \sin\theta = \theta$$

Splitting into an unperturbed and a perturbed Hamiltonian

$$\mathcal{H} = \mathcal{H}_o + \mathcal{H}'$$

$$\mathcal{H} = \begin{pmatrix} \frac{3}{2}\beta_o g_{\parallel} H+D & 0 & 0 & 0 \\ 0 & \frac{1}{2}\beta_o g_{\parallel} H-D & 0 & 0 \\ 0 & 0 & -\frac{1}{2}\beta_o g_{\parallel} H-D & 0 \\ 0 & 0 & 0 & -\frac{1}{2}\beta_o g_{\parallel} H+D \end{pmatrix}$$

$$+ \begin{pmatrix} -\frac{3}{4}\beta_o g_{\parallel} H\theta^2 & \frac{\sqrt{3}}{2}\beta_o g_{\perp} H\theta & 0 & 0 \\ \frac{\sqrt{3}}{2}\beta_o g_{\perp} H\theta & -\frac{1}{4}\beta_o g_{\parallel} H\theta^2 & \beta_o g_{\perp} H\theta & 0 \\ 0 & \beta_o g_{\perp} H\theta & \frac{1}{4}\beta_o g_{\parallel} H\theta^2 & \frac{\sqrt{3}}{2}\beta_o g_{\perp} H\theta \\ 0 & 0 & \frac{\sqrt{3}}{2}\beta_o g_{\perp} H\theta & \frac{3}{4}\beta_o g_{\parallel} H\theta^2 \end{pmatrix}$$

The zero angle unperturbed energies are:

$$E_{o1} = {}^{3}/_{2}\,\beta_o\, g_{\parallel} H + D$$

$$E_{o2} = {}^{1}/_{2}\,\beta_o\, g_{\parallel} H - D$$

$$E_{o3} = -{}^{1}/_{2}\,\beta_o\, g_{\parallel} H - D$$

$$E_{o4} = -{}^{3}/_{2}\,\beta_o\, g_{\parallel} H + D$$

The perturbed energies are obtained using:

$$E'_k = \mathcal{H}'_{kk} + \sum_{\substack{\ell=1 \\ \ell \neq k}}^{4} \frac{\mathcal{H}'_{\ell k}\,\mathcal{H}'_{k\ell}}{E_{ok} - E_{o\ell}}$$

$$E'_1 = -\frac{3}{4}\,\beta_o\, g_{\parallel} H\,\theta^2 + \frac{{}^{3}/_{4}(\beta_o\, g_{\perp} H\,\theta)^2}{\beta_o\, g_{\parallel} H + 2D}$$

$$= -\frac{3}{4}\,(g_{\perp}\beta_o\, H)\left(\frac{g_{\parallel}}{g_{\perp}} - \frac{\beta_o\, g_{\perp} H}{\beta_o g_{\parallel} H + 2D}\right)\theta^2$$

$$E'_2 = -\frac{1}{4}\,\beta_o\, g_{\parallel} H\,\theta^2 + \frac{{}^{3}/_{4}(\beta_o\, g_{\perp} H\,\theta)^2}{-\beta_o\, g_{\parallel} H - 2D} + \frac{(\beta_o\, g_{\perp} H\,\theta)^2}{\beta_o\, g_{\parallel} H}$$

$$= -\frac{1}{4}\,(g_{\perp}\,\beta_o\, H)\left(\frac{g_{\parallel}}{g_{\perp}} + \frac{3\beta_o\, g_{\perp} H}{\beta_o\, g\ H + 2D} - \frac{4g_{\perp}}{g_{\parallel}}\right)\theta^2$$

$$E'_3 = \frac{1}{4}\,\beta_o\, g_{\parallel} H\,\theta^2 + \frac{(\beta_o\, g\ H\,\theta)^2}{-\beta_o\, g\ H} + \frac{{}^{3}/_{4}\,(\beta_o\, g\ H\,\theta)^2}{\beta_o\, g\ H - 2D}$$

$$= \frac{1}{4}\,(\beta_o\, g_{\perp} H)\left(\frac{g_{\parallel}}{g_{\perp}} - \frac{4g_{\perp}}{g_{\parallel}} + \frac{3\beta_o\, g_{\perp} H}{\beta_o\, g_{\parallel} H - 2D}\right)\theta^2$$

$$E_4' = \frac{3}{4}\beta_o g_{\parallel} H \theta^2 + \frac{3/4(\beta_o g_{\perp} H \theta)^2}{-\beta_o g_{\parallel} H + 2D}$$

$$= \frac{3}{4}(\beta_o g_{\perp} H)\left(\frac{g_{\parallel}}{g_{\perp}} - \frac{\beta_o g_{\perp} H}{\beta_o g_{\parallel} H - 2D}\right)\theta^2$$

The energies are, thus, to second order approximation

$$E_1 = \frac{3}{2}\beta_o g_{\parallel} H + D - \frac{3}{4} g_{\perp} \beta_o H \left(\frac{g_{\parallel}}{g_{\perp}} - \frac{\beta_o g_{\perp} H}{\beta_o g_{\parallel} H + 2D}\right)\theta^2$$

$$E_2 = \frac{1}{2}\beta_o g_{\parallel} H - D - \frac{1}{4} g_{\perp} \beta_o H \left(\frac{g_{\parallel}}{g_{\perp}} + \frac{3\beta_o g_{\perp} H}{\beta_o g_{\parallel} H + 2D} - \frac{4g_{\perp}}{g_{\parallel}}\right)\theta^2$$

$$E_3 = -\frac{1}{2}\beta_o g_{\parallel} H - D + \frac{1}{4} g_{\perp} \beta_o H \left(\frac{g_{\parallel}}{g_{\perp}} + \frac{3\beta_o g_{\perp} H}{\beta_o g_{\parallel} H - 2D} - \frac{4g_{\perp}}{g_{\parallel}}\right)\theta^2$$

$$E_4 = -\frac{3}{2}\beta_o g_{\parallel} H + D + \frac{3}{4} g_{\perp} \beta_o H \left(\frac{g_{\parallel}}{g_{\perp}} - \frac{\beta_o g_{\perp} H}{\beta_o g_{\parallel} H - 2D}\right)\theta^2$$

The two desired frequencies are:

$$\nu_{1-2} = \frac{E_1 - E_2}{h}$$

$$= \frac{\beta_o}{h} g_{\parallel} H + \frac{2D}{h} - \frac{1}{2}\frac{\beta_o}{h} g_{\perp} H \left(\frac{g_{\parallel}}{g_{\perp}} + \frac{2g_{\perp}}{g_{\parallel}} - \frac{3\beta_o g_{\perp} H}{\beta_o g_{\parallel} H + 2D}\right)\theta^2$$

$$\nu_{2-3} = \frac{E_2 - E_3}{h}$$

$$= \frac{\beta_o}{h} g_{\parallel} H - \frac{1}{2}\frac{\beta_o}{h} g_{\perp} H \left(\frac{g_{\parallel}}{g_{\perp}} - \frac{4g_{\perp}}{g_{\parallel}} + \frac{3(\beta_o H)^2 g_{\perp} g_{\parallel}}{(\beta_o g_{\parallel} H)^2 - 4D^2}\right)\theta^2$$

APPENDIX II

Weighting Factors for Ninety Degree Data

The following weighting factor equations are for an intersection of two straight lines which have the same thickness representing experimental uncertainty. Therefore, the two assumptions which are made concerning the actual ninety degree, $g_\perp$ versus D, curves are that over the interval between known points the curves are straight lines and that all the curves have the same experimental error thickness. The first assumption is very good since the curves are nearly straight over 30 times the smallest interval, and the second assumption was verified to be satisfactory by computing the actual uncertainties in $g_\perp$ and D for all the curves. One factor remains arbitrary, which is the relative sizes of the D and $g_\perp$ scales to each other. In order to get the most variation among the weighting factors and to use scales which make the error bars for $g_\perp$ and D about the same length, the D scale in Kmc/sec has to be 1/10th the size of the $g_\perp$ scale.

Based on the foregoing statements the following is developed. Figure 8 shows the geometrical relationships.

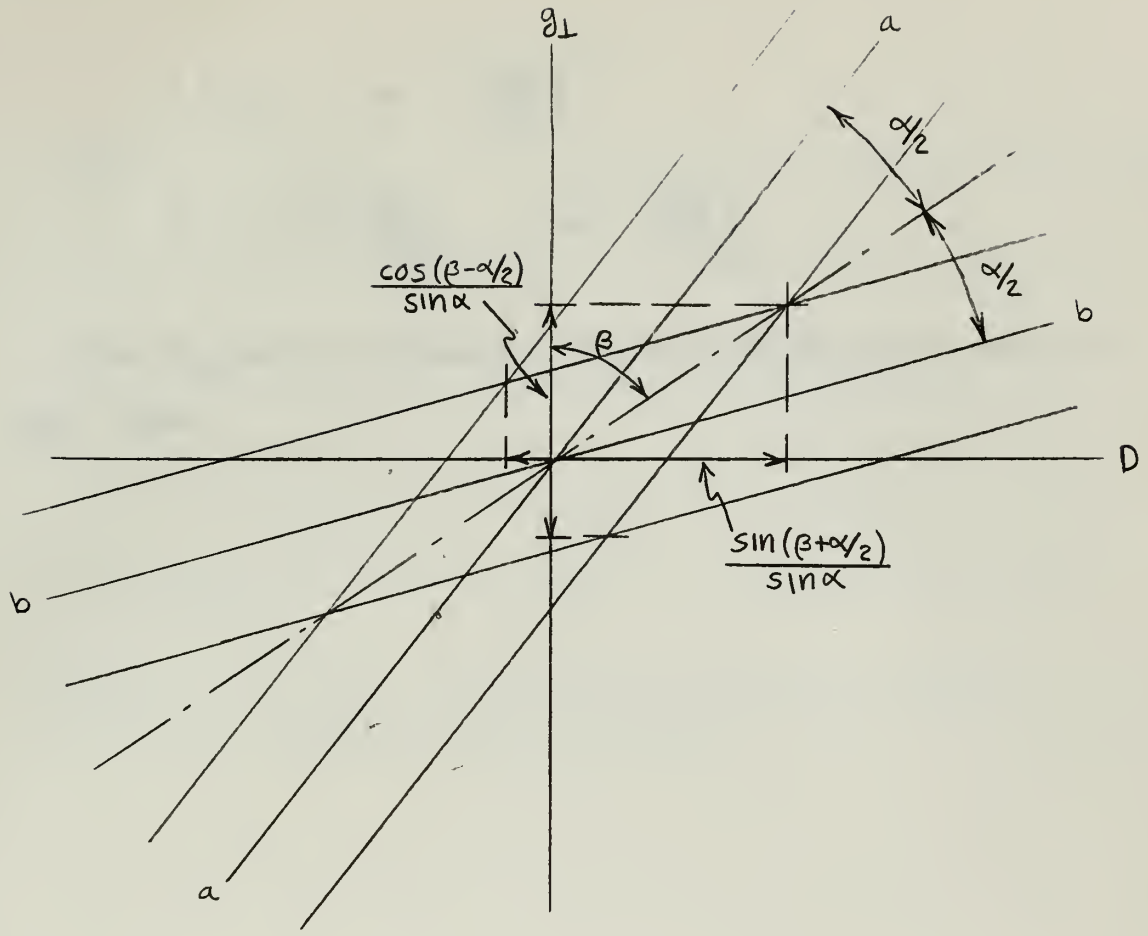

Figure 8. Intersection of Two data lines having unit width

From figure 8:

Weighting factor for intersection value of $g_\perp$ equals:

$$W(g_\perp) = \frac{\sin\alpha}{\cos(\beta - \alpha/2)}$$

And for intersection value of D:

$$W(D) = \frac{\sin\alpha}{\sin(\beta + \alpha/2)}$$

In terms of the slopes of the two lines

$$\beta - \alpha/2 = \tan^{-1}\left(\frac{\Delta D}{\Delta g_\perp}\right)_a$$

$$\beta + \alpha/2 = \tan^{-1}\left(\frac{\Delta D}{\Delta g_{\perp}}\right)_b$$

$$\alpha = \tan^{-1}\left(\frac{\Delta D}{\Delta g_{\perp}}\right)_b - \tan^{-1}\left(\frac{\Delta D}{\Delta g_{\perp}}\right)_a$$

The $\Delta g_{\perp}$ and ΔD values are obtained from the data in table II ($\Delta g_{\perp} = .001$)

BIBLIOGRAPHY

1. Bleaney, E. and K. W. H. Stevens, "Paramagnetic Resonance", Rep. Prog. Physics, 16, 108, 1953.

2. Bowers, K. D. and J. Owen, "Paramagnetic Resonance II", Rep. Prog. Physics, 18, 304, 1955.

3. Geusic, J. E. "Paramagnetic Fine Structure Spectrum of Cr^{+++} in Single Ruby Crystal", Phys. Rev., Vol. 102, June 1, 1956.

4. Manenkov, A. A. and A. M. Prokhorov, Soviet Physics JETP1, 611, 1955

5. Pake, G. E., "Paramagnetic Resonance", W. A. Benjamin, Inc., 1962.

6. Varian Associates, Instruction Manual for V-4502 EPR Spectrometer Systems (Pg. 5-16)

7. Weaver, H., "Some Useful Steps in the Development of the Spin Hamiltonian Suitable for Analyzing EPR Data", Varian Associates Report, Seventh Annual NMR-EPR Workshop, Nov. 1963.